Simulation of the Effect of Noncrystalline Species on Long Spacing in Crystalline/Noncrystalline Polymer Blends

K. M. Kit*,† and J. M. Schultz

Department of Materials Science and Engineering, University of Delaware, Newark, Delaware 19716

Received June 5, 2002; Revised Manuscript Received September 10, 2002

ABSTRACT: A finite element model is used to predict the effect of composition on long spacing (L) in blends of crystalline and noncrystalline polymers. In this model, the diffusive transport of noncrystallizable moieties away from the crystals from which they are excluded is tracked. The effect of the local concentration of noncrystallizable material near the growing interface on the kinetics of crystallization is modeled. Parameters in the model are the Peclet number (Pe), the linear crystallinity (ϕ_c), and the overall concentration of noncrystallizable molecules (C_o). The overall crystallization rate (T) depends on these three parameters. T is found to exhibit a maximum (T_{max}) with respect to ϕ_c at given C_o and Pe. It is shown that, over a considerable range of Pe and C_o, T_{max} exhibits either a nearly constant low value nor a nearly constant higher value. It is suggested that T_{max} is the operating condition for such crystallization. From this hypothesis, expected values of long spacing are predicted. The dependence of L on C_o is found to lie on either of two branches, depending on the value of Pe. Large Pe shows a small effect of C_o on L, while high Pe exhibits a relatively large effect. These results agree with observations on blend systems.

Introduction

When a blend of a crystallizable polymer and a noncrystallizable polymer is crystallized quiescently, the noncrystallizable moiety can be redistributed to any of the following places: between lamellae, between growth arms (lamellar bundles), or between spherulites. A question is, "what controls the distribution of the noncrystallizable polymer?" The answer to this question should depend on the relative kinetics of crystallization and molecular diffusion.[1,2]

Let us refer to the noncrystallizable moiety as B. In general, if B were excluded to any degree from the growing spherulite, its concentration would build in the melt near the growth surface and continuously alter (usually reduce) the growth velocity. However, the general experimental finding is that spherulites in such blends grow at a constant velocity (see, e.g., refs 3−17), indicating that steady state is attained. In this case, there can be no difference in the concentration of B on either side of the growth front; the excluded B must lie within the spherulite, either between crystalline lamellae or between growth arms.

Conceptually, one can begin to understand the situation in terms of the diffusion length $\delta = D/V$, where D is the diffusivity of the noncrystallizable species in the blend and V is the velocity of the crystallization front. The diffusion length is a measure of the extent of the compositional field (for the excluded B) ahead of the propagating interface. If δ is significantly smaller than the lateral dimension of the growing body (lamella or growth arm), then the extent to which the crystal-excluded B can escape laterally (normal to the growth direction) from the growing body is restricted; its diffusive motion becomes largely one-dimensional, parallel to the growth direction. The concentration of B ahead of the interface, in this case, will build up, and steady state cannot be attained. If δ is comparable with or somewhat larger than the lateral dimension of the growing body, then the excluded B can diffuse laterally and can finally be trapped between growing bodies. If δ is considerably larger than the lateral extent of the growing body, B molecules move large distances from the growing bodies and are neither localized in the melt near the growing interface nor trapped between the bodies.

Considering first the lamellar level, if δ is comparable to the lamellar thickness L_c, then the random-walk, center-of-mass diffusion of B molecules requires that some portion of the excluded B find itself in the noncrystalline region separating the lamellae. At steady state, and if all redistribution were to occur at this structural level, then the average concentration of B within the lamellar stacking must be identical to the overall concentration of B. However, the interlamellar spaces, where this material is to be found, can be wider or narrower, depending on how far, on average, a B molecule has moved. Molecules of the crystallizable material, termed A, add from the melt to the B in these spaces, such that the overall concentration of A and of B are identical on both sides of the growth front. For small values of δ, the range of diffusion into the interlamellar regions is small, and consequently the interlamellar region is narrow and contains relatively little A. As δ becomes larger, this space opens up and the concentration of A in the interlamellar space increases.

As δ increases still more, the interlamellar spaces become wider and the concentration of A in these regions becomes comparable to the overall composition. In this case, it is likely that crystallization will occur in these regions, effectively thwarting the interlamellar redistribution process and requiring that B be distributed into the more widely spaced regions between growth arms.

† Present address: Department of Materials Science and Engineering, University of Tennessee, Knoxville, TN 37996-2200.

* To whom correspondence should be addressed: e-mail kkit@utk.edu; Tel 865-974-7055.

10.1021/ma020875t CCC: $22.00
Published on Web 11/21/2002

In the conceptual model just described, the interlamellar spacing L is an important parameter, and one is led to infer that a Peclet number $Pe = LV/D = L/\delta$ might be an appropriate index for the distribution of B in the final product.

In the following, we present a finite element model designed to simulate the distribution of B in front of a stack of lamellae and to quantify the condition for trapping B between lamellae. The model allows redistribution of B only between crystalline lamellae and does not attempt to define the conditions under which interarm redistribution is favored. (It is useful to mention, however, that interarm segregation has also been treated[18] using the finite element model described in the next section.) This method has been used previously to simulate the growth of finite[19] and infinite[20] stacks of polymer lamellae. This previous work addressed the kinetics of crystallization and the development of fibrils while the present work describes how these kinetics may affect the development of the long period in a stack of growing polymer lamellae.

The Method

The finite element simulation is a modification of the method described by Kit and Schultz.[21] In this method, the position of a set of platelike crystals, stacked periodically, is followed by solving the diffusion equation in the melt in front of each crystal. The overall volume fraction of B is taken as C_o. The problem is reduced to three dimensions, two of which are spatial (the stacking direction and the growth direction) and the third of which is time. At each step, the concentration of B at the crystal−melt interface feeds back to determine the growth velocity in the next time step.

The velocity at each step is governed by C^*, the steady-state concentration of B in the melt at the growing interface. C^* alters the growth velocity from what it would be for a pure melt of the crystallizable species. On can write, in general, for the growth velocity,[2]

$$V(T,C^*) = A(T)[1 - C^*] \exp\left\{-\left[\frac{B(T)}{T(T_m - T)}\right]\right\} \quad (1)$$

where $A(T)$ contains a mobility term, T_m is the actual melting point for the crystal near the growth surface, and $B(T)$ is a Hoffman−Lauritzen term[22] of the form

$$B(T) = \frac{\lambda b_1 T_m \sigma_s \sigma_e}{k_B T \Delta h_f} \quad (2)$$

where λ is a constant of order unity, b_1 is the interchain spacing in the growth direction, T_m is the melting point of the twisted crystal, σ_s is the surface energy of the growth face, σ_e is the surface energy of the broad surfaces of the lathlike crystal, k_B is Boltzmann's constant, and Δh_f is the enthalpy of fusion. Changes in C^* can affect $A(T)$, T_m, Δh_f, and the surface energies. However, for very similar crystallizable and poorly crystallizable species (e.g., chains of similar chemistry but different tacticity, defect concentration, or molecular mass), there will be little change in T_m and Δh_f, and only molecular mass would markedly affect $A(T)$. In the following, we shall assume a blend in which the concentration of poorly crystallizable species at the front affects the growth velocity only through the $[1 - C^*]$ term, representing the dilution of crystallizable species in the melt near the growth front.

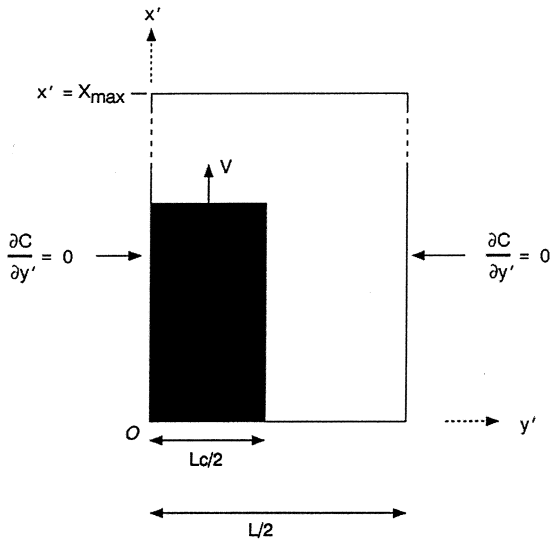

Figure 1. Solution domain for simulation of growth of an infinite stack of lamellar crystals.

Figure 1 shows the unit cell of the system being modeled. A periodic, infinite stack of crystals will be simulated by imposing periodic boundary conditions on the left and right edges ($y' = 0$ and $y' = L/2$). L is the periodicity, and L_c is the thickness of each crystal. Since the system is periodic, one need solve only one unit cell of the system. Here, the blackened area indicates the half-thickness of the crystal, with the centerline at $y' = 0$. The cell boundary at $y' = L/2$ is at the midline of lateral region between crystals. The crystal grows with velocity V in the x'-direction.

The periodicity dictates the boundary conditions $\partial C/\partial y' = 0$ at $y' = 0$ and $y' = L/2$. The same condition is imposed along the lateral side of the growing crystal to simulate an insulated boundary. The insulating condition $\partial C/\partial x' = 0$ is imposed at $x' = 0$ and at $x' = X_{max}$. The magnitude of X_{max} was always large enough so that this boundary was effectively at infinity (i.e., C never rose above C_o). The boundary condition at growing crystal fronts is

$$C^*V = D\left(\frac{\partial C}{\partial x'} + \frac{\partial C}{\partial y'}\right) \quad (3)$$

This ensures mass conservation (i.e., the flux of rejected species, C^*V, diffuses into the surrounding melt). At each time step, C^* is determined by averaging the solute concentration, C, along the length of this boundary. The mesh used for the solution is described in ref 21.

The real spatial and time variables are x', y', and t'. In the finite element analysis, a set of nondimensional variables is used. These are

$$x = \frac{x'}{D/V}, \quad y = \frac{y'}{L_c}, \quad t = \frac{t'}{D/V^2} \quad (4)$$

Additionally, the linear degree of crystallinity is given by

$$\phi_c = \frac{L_c}{L} \quad (5)$$

Each simulation solves the Fickian diffusion equation over the domain described above for a series of time

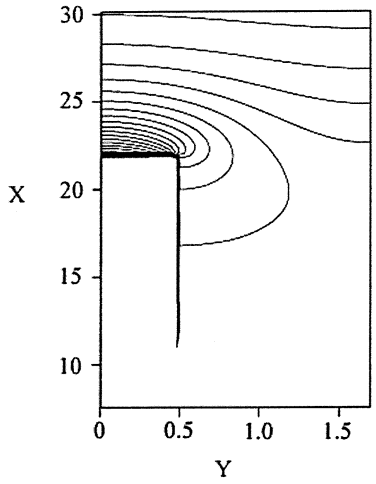

Figure 2. Contour plot of diluent concentration surrounding a growing lamellar crystal (t = 100, Pe = 5, C_o = 0.5, ϕ_c = 0.3).

steps. Simulations are uniquely determined by the following parameters: Pe, ϕ_c, and C_o. The computer program outputs the following data for each simulation: interface concentration and position (C^* and X^*) as a function of time and the entire concentration field, $C(x,y)$, at the end of the simulation. To explore the effects of ϕ_c (and hence L) on crystallization kinetics, ϕ_c was varied for fixed L_c and Pe. Recall that the reduced y-dimension is scaled by L_c so that the crystal thickness was always 1. This series of simulations was repeated for several different Peclet numbers to provide the necessary data.

A typical contour plot of $C(x,y)$ is shown in Figure 2 for $Pe = 5.0$, $\phi_c = 0.3$, and $C_o = 0.5$ The lamella occupies the region $0 \le y \le 0.5$, $0 \le x \le 22.1$ and has grown in the x-direction for 100 time units. Note that the contour lines intersect the symmetric boundaries ($y = 1.667$ and $y = 0$) at right angles. This is a check that the symmetric boundaries were formulated correctly. Note also that the contour lines outline the boundary of the crystal because the concentration changes steeply to zero at the crystal boundaries. Figure 2 only shows a portion of the solution domain, and the insulating conditions at $x' = 0$ and at $x' = X_{max}$ are not shown. We have assumed Fickian diffusion here, but the incorporation of reptation effects may be necessary depending on the time scales involved in the simulation and the reptation time of the polymers of interest. The results of the current model show, at least to a first approximation, that crystallization kinetics may affect the determination of long period.

Results

Effects of the Process on the Concentration of B. The effect of Pe on the evolution of the concentration C of B in reduced time is shown in Figure 3 for $C_o = 0.5$ and $\phi_c = 0.3$. It is seen that C^* rises quickly from C_o and then tends toward a constant value at longer times. When Pe is large, C_o rises more quickly initially, begins to level off sooner, and tends toward a higher steady-state value than when Pe is small. Recall that $Pe = VL_c/D$ and that real time, t', equals tD/V^2, where t is the reduced time. Therefore, the time scales for the curves in Figure 2 are directly comparable if changes in Pe reflect only changes in L_c and not changes in D or V.

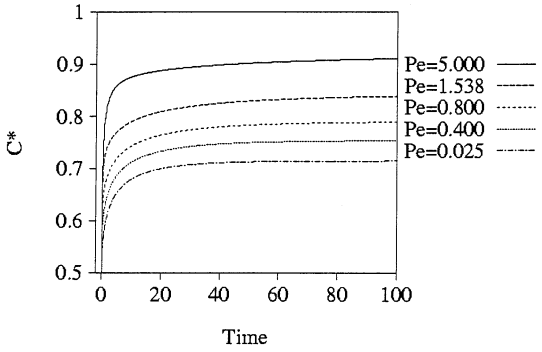

Figure 3. Effect of Pe on the evolution of C^* ($C_o = 0.5$, $\phi_c = 0.3$).

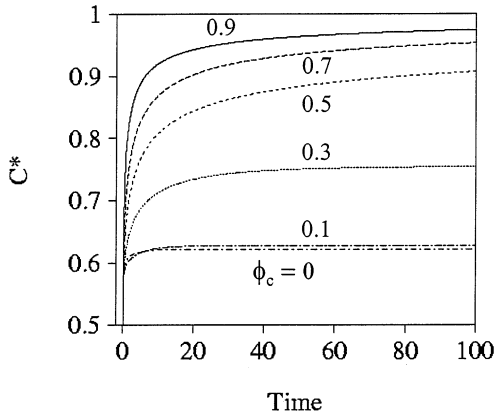

Figure 4. Effect of ϕ_c on the evolution of C^* ($C_o = 0.5$, $Pe = 0.4$).

In order for a steady state to be reached, the rate at which noncrystallizable species (B) are excluded must equal the rate at which they can diffuse normal to the growth direction. As L_c is increased while D and V are kept constant (Pe increases), excluded chains must diffuse further in order to reach the amorphous region separating the lamellae. This results in a faster initial increase in C^*, relative to thinner lamellae. The larger steady-state value of C^* develops in order to provide a concentration gradient large enough to allow B to maintain the required flux of B from the growing lamella. Likewise, an increase in Pe due to lower D or greater V results in slower diffusion or faster solute expulsion and has a similar effect.

The effect of ϕ_c on the time dependence of C^* is shown in Figure 4 for $C_o = 0.5$ and $Pe = 0.4$. Since Pe is kept constant for these simulations, changes in ϕ_c must be interpreted as changes in the long period, L. The curve for $\phi_c = 0$ is the result for a single lamella growing in an infinite melt and was achieved by using a very large value of L. The results for $\phi_c = 0.1$ are very similar to the results for the single lamella. This indicates that there is very little interaction between neighboring lamellae when $\phi_c = 0.1$ and $Pe = 0.4$. As ϕ_c increases, the distance between neighboring lamellae decreases, and the diffusion fields begin to overlap significantly. This leads to an increase in the steady-state value reached by C^*.

In some situations there is a limiting value of ϕ_c above which steady-state growth should not be possible for the present problem. In order for a steady state to develop, a net transport of B parallel to the growth direction must not be necessary. Recall that no B is incorporated into the crystalline lamellae. To avoid net mass trans-

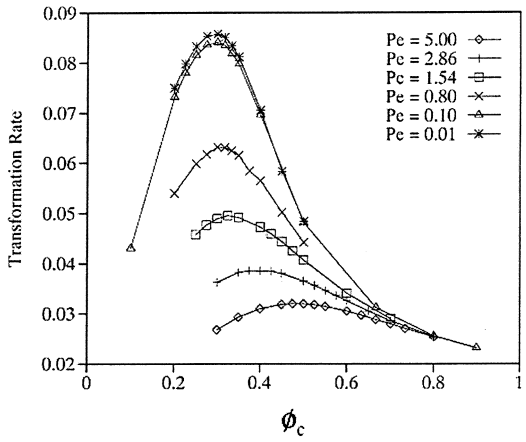

Figure 5. Crystalline volume transformation rate as a function of ϕ_c for several values of Pe ($C_o = 0.5$).

port parallel to the growth direction, the A fraction behind the growth front cannot exceed the overall A fraction $1 - C_o$. Therefore, a steady growth rate will develop for the present problem only when the condition $\phi_c \leq 1 - C_o$ is satisfied. Referring to the results in Figure 4, which were generated with $C_o = 0.5$, steady-state growth will not develop when ϕ_c is greater than 0.5. There, it appears that a steady state has been reached after 100 time units for $\phi_c = 0.0$, 0.1, and 0.3, but not for $\phi_c = 0.5$, 0.7, or 0.9.

Steady-State Transformation Rate. We describe first the concept used. The rate at which mass is transformed from melt to crystal is proportional to $(L_c/L)V$ or $\phi_c V$. It is not difficult to show that V is greatest when the crystals are thinnest ($\phi_c \rightarrow 0$), but in this case the mass transformed is very small. At the opposite extreme, as $\phi_c \rightarrow 1$, the mass transformed is 100%, but the growth velocity is very small, since all B must diffuse away parallel to the growth direction (a one-dimensional diffusion situation). The most rapid rate of mass transformation occurs somewhere between these extremes. In the following, we take the operating point to be the value of ϕ_c which gives the maximum rate of mass transformation.

Computed transformation rates, $T = \phi_c V$, are plotted vs ϕ_c ($=L_c/L$) in Figure 5 for several values of Pe and with $C_o = 0.5$. For each simulation, the value of C^* at $t = 100$ is used to identify the steady-state interface velocity in the calculation of T. As expected, T goes to zero at $\phi_c = 0$ and to a very low value at $\phi_c = 1$. Also, as expected, T exhibits a maximum at some ϕ_c^* between these extremes. The position of this maximum shifts toward lower values of ϕ_c as Pe increases. When Pe is small, the field of B surrounding a growing crystal is quite broad, and the maximum transformation rate will occur at relatively small values of ϕ_c. As Pe increases, the diffusion fields become smaller, and the crystals must be brought closer together before they start to significantly affect each others growth, conceptually explaining the observed increase of the maximum with Pe. Note also that the magnitude of the maximum transformation rate decreases as Pe is increased. Since an increase in Pe causes a general increase in C^* (see Figure 3), it also causes a decrease in the overall kinetics.

The position of the maximum transformation rate shifts also as C_o changes. Computed transformation rates vs ϕ_c are plotted in Figure 6 for several values of C_o, with $Pe = 0.1$. As C_o is increased, ϕ_c^* shifts to lower

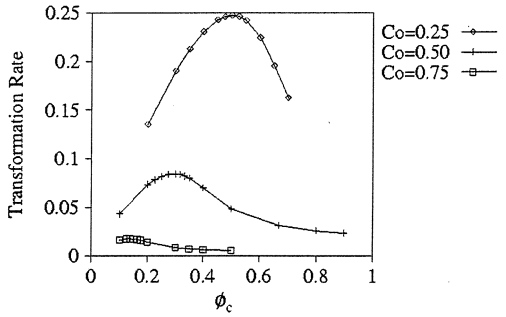

Figure 6. Crystalline volume transformation rate as a function of ϕ_c for several values of C_o ($Pe = 0.1$).

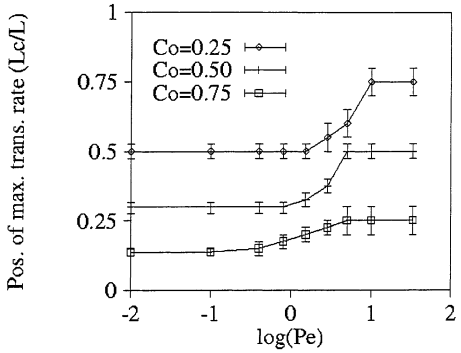

Figure 7. Position of maximum transformation rate as a function of Pe for several values of C_o.

values of ϕ_c, and the magnitude of the maximum decreases. ϕ_c^* decreases as C_o increases in order for the noncrystallizing species to be incorporated between the lamellae.

Discussion

Many simulations were run in order to determine the effect of Pe and C_o on the position of the maximum transformation rate. The results of all of these simulations are shown in Figure 7. It should be pointed out that each point in this figure is a result from a different simulation. The points in Figure 7 are the values of ϕ_c for which the mass transformation rate was found to be the highest for the given Pe and C_o. The accuracy to which each maximum could be determined was dependent on the number of simulations carried out in the vicinity of the maximum. The error bars in Figure 7 represent the values of ϕ_c closest to the maximum for which the transformation rate was determined numerically.

Figure 7 shows the value of ϕ_c^*, the position of the maximum steady-state transformation rate, as a function of Pe for three values of C_o. It is seen that the position of the maximum transformation rate varies only over a narrow range of Peclet number. It increases as Pe is increased in the range from 0.1 to 10. Below $Pe = 0.1$, ϕ_c^* remains constant. As Pe approaches 10, ϕ_c^* approaches the limit $1 - C_o$, above which steady-state growth is not possible, and ϕ_c^* will remain at this level as Pe is increased further. It is interesting to note that ϕ_c^* changes only over a narrow range of Pe.

The reason for the plateau at low Peclet numbers will now be discussed. Compare the transformation rates for $Pe = 0.01$ and $Pe = 0.1$ shown in Figure 5. Not only are the positions of the maxima very similar but the magnitudes of the transformation rates as well. The distance between a growing crystal and the periodic

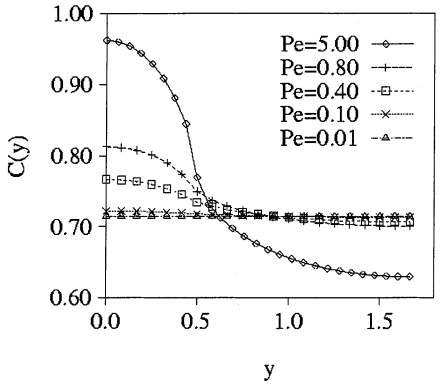

Figure 8. Concentration profiles, $C(x = X^*, y)$ at $t = 100$ for $\phi_c = 0.3$ and varying Peclet number.

boundary condition is approximately equal to half of the reduced long period, $L/2$ (see Figure 1). When δ is much greater than $L/2$ (i.e., $Pe \ll 2$), concentration gradients in the y direction should disappear. This can be seen in Figure 8, which shows the concentration gradients in the y direction at the x position of the growth front for different Peclet numbers. When $Pe = 0.1$ and 0.01, the concentration gradients in the y direction are virtually flat. Therefore, changes in Pe should not have much of an effect on the results as long as $Pe \ll 2$, and ϕ_c^* will be independent of the Pe number when it is sufficiently small.

It has been reported for several miscible binary blends[23−28] that the long period L is a function of the overall concentration, C_o, of noncrystallizing species. This behavior has been interpreted by some[25,27,29] as proof of interlamellar incorporation of noncrystallizable species. However, there has been no attempt to propose a quantitative relationship between L and C_o.

Assuming the maximum crystalline volume transformation rate as an operating point, the results of the previous section can be used to predict long periods in miscible blends. The long period will be a function of the overall impurity concentration and the Peclet number. Actually, it is the quotient L/L_c which is predicted, but since L_c is taken as known, L is the effective variable. The minimum long period, L_{min}, is limited by the maximum linear degree of crystallinity, ϕ_c^{max}, which is limited by the value of $(1 - C_o)$:

$$L^{min} = \frac{L_c}{\phi_c^{max}} = \frac{L_c}{1 - C_o} \qquad (6)$$

This dependence of L on C_o will result for large Peclet numbers, where ϕ_c^* is limited by $(1 - C_o)$. L will increase as Pe decreases. The variation of ϕ_c^* with Pe is shown in Figure 7 for three values of C_o. It was explained previously that ϕ_c^* is constant for Pe less than 0.1. Therefore, to get an upper bound on L/L_c as a function of C_o, additional simulations were carried out with $Pe = 0.01$ for several values of C_o besides those in Figure 7.

Figure 9 shows several sets of L/L_c vs C_o data from the literature.[26−28,30] In all of these cases, the increase in L with increasing C_o is largely due to increases in the amorphous layer thickness, L_a, while lamellar thickness, L_c, is relatively independent of C_o. In two of the cases (iPP/PCP,[26] PCL/SAN[30]), L_c actually decreases slightly while both L_a and L increase. For the other blends (PBT/Par,[27] PEO/PMMA,[28] PCL/PVME[30]), the

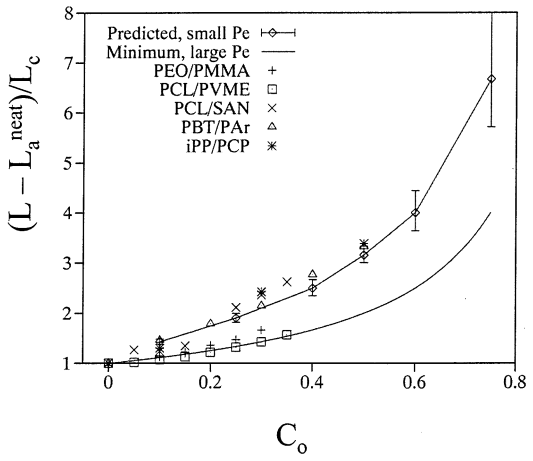

Figure 9. Predicted and actual reduced long periods as a function of C_o.

increase in L_a with increasing C_o is at least 6 times greater than the increase in L_c. Also shown in that figure are the minimum possible L, as calculated by (6), and the maximum L (corresponding to $Pe = 0.01$), shown as the upper solid line. The predicted value of L/L_c goes to 1 for homopolymers ($C_o = 0$). However, in reality, neat polymers have a linear crystallinity less than 1 (i.e., some portion of the crystallizable polymer resides in the amorphous layers separating the crystalline lamellae). The noncrystalline B molecules excluded from the crystals would add to the A molecules already resident between the crystals and would expand the thickness of those layers beyond the initial, neat polymer value. Therefore, the long period data from the literature was corrected for a nonzero value of L_a at $C_o = 0$. The data points in Figure 9 are $(L - L_a^{neat})/L_c$, where L is the measured long period, L_a^{neat} is the measured amorphous layer thickness in the neat homopolymer, and L_c is the measured lamellar thickness.

It is seen in Figure 9 that the data for polycaprolactone/poly(vinyl methyl ether) and poly(ethylene oxide)/poly(methyl methacrylate) lie very close to the minimum possible long periods (prediction for large Peclet numbers). The data for the other three blends lie very close to the predicted long periods for small Pe. Peclet numbers will be estimated for two of these blend systems: poly(ethylene oxide)/poly(methyl methacrylate) (PEO/PMMA) and isotactic polystyrene/polycyclopentadiene (iPP/PCP). The PEO/PMMA data shown in Figure 9 were reported by Talibuddin et al.[28] for a crystallization temperature of 45 °C. The weight-average molecular weights of the PEO and PMMA used were 144 000 and 64 000, respectively. Talibuddin et al. reported $L_c = 20$ nm and $V = 1060$ nm/s for PEO at 45 °C. The self-diffusion coefficient for PEO at this molecular weight and temperature can be determined by extrapolating data reported by Cheng et al.[31] This results in a diffusion coefficient of 3×10^{-11} cm^2/s. This will be taken as an upper bound on the interdiffusion coefficient of the blend, since the mobility of PMMA segments is much less than that of PEO segments[32] and the molecular weights of the PEO and PMMA are relatively close. This leads to a lower bound of 7 for the Peclet number of this blend. Note that the PEO/PMMA data in Figure 9 agrees well with the prediction for large Pe (5.0).

The iPP/PCP data shown in Figure 9 was reported by Martuscelli et al.[26] for a crystallization temperature

of 123 °C. The weight-average molecular weights of the iPP and PCP used were 300 000 and 630, respectively. Martuscelli et al. reported $L_c = 10$ nm, and Keith and Padden[33] reported $V = 333$ nm/s for iPP at 123 °C. The diffusivity of PCP in iPP has not been reported, and it must be estimated using the reported diffusivity of benzene in iPP. The PCP used by Martuscelli et al.[26] had a degree of polymerization of 10 and is far below the entanglement limit. Therefore, the diffusivity D is given by the Rouse model:[34]

$$D = \frac{kT}{\zeta_0 N} \tag{7}$$

where k is Boltzmann's constant, T the absolute temperature, ζ_0 the friction coefficient of the monomer, and N the degree of polymerization. The diffusivity of the cyclopentadiene monomer is then given by kt/ζ_0 ($N = 1$). A lower bound on the diffusivity of cyclopentadiene in iPP is given by the diffusivity of benzene in iPP, since cyclopentadiene is structurally similar to benzene and somewhat smaller. Flynn[35] has reported the diffusivity of benzene in iPP at 30 °C to be 1.7×10^{-9} cm^2/s. The activation energy for diffusion of benzene in polyethylene is 28 kJ/mol.[36] This is also a reasonable value for the activation energy for diffusion of benzene in polypropylene.[35] Using this activation energy, the diffusivity of benzene in polypropylene at 123 °C is calculated to be 6.3×10^{-7} cm^2/s. This is taken as a lower bound to the diffusivity of cyclopentadiene (kt/ζ_0) in iPP at 123 °C. The diffusivity of PCP with a degree of polymerization of 10 then found to be 6.3×10^{-8} cm^2/s. This leads to an upper bound of 0.013 for the Peclet number in this system at 123 °C. Note that the iPP/PCP data in Figure 9 agrees well with the prediction for small Peclet numbers (0.1).

The observation that the data points in Figure 9 lie close to the upper and lower predictions and not in between is not surprising, in light of the small range of Peclet numbers for which ϕ_c* varies between the maximum and minimum. This result is consistent with the apparent experimental observation that the long spacing either expands markedly with concentration of noncrystallizing species or varies little from the value for the neat polymer. These extremes now appear to be related to Peclet numbers above or below unity, above indicating a small diffusion length and below indicating a large diffusion length.

Summary

The diffusional transport of noncrystallizable material away from the crystallization front of a system of growing, periodically stacked crystalline lamellae has been simulated, using a finite element model. The effect of the localized compositional field on the growth velocity and overall transformation rate of the material is the output of the model. The Peclet number (*Pe*), the overall composition (C_o), and the linear crystallinity (ϕ_c) are variables in the simulation. It is shown that the overall transformation rate exhibits a maximum with respect to ϕ_c, the position of that maximum increasing with increasing *Pe* and decreasing C_o. Assuming the maximum volume crystallization rate to be the operating principle, the expected optimal values ϕ_c of as a function of *Pe* and C_o are predicted. It is shown that for any given C_o the maximum transformation rate is effectively constant for *Pe* below a value of approximately 1 and assumes another, higher effectively constant value for Peclet numbers above approximately 5. The dependences of long spacing on C_o are accordingly expected to lie on either of two curves, corresponding to high and low Peclet numbers (little change of long spacing or large long spacings which track C_o, respectively), and this result accords with experimental observation.

Acknowledgment. This research was supported by the National Science Foundation under Grant DMR-9115308.

References and Notes

(1) Schultz, J. M. *Polymer* **1991**, *32*, 3268.
(2) Schultz, J. M. *Polymer Crystallization*; Oxford University Press: Oxford, UK, 2001.
(3) Keith, H. D.; Padden, F. J., Jr., *J. Appl. Phys.* **1964**, *35*, 1286.
(4) Wang, T. T.; Nishi, T. *Macromolecules* **1977**, *10*, 421.
(5) Ong, C. J.; Price, F. P. *J. Polym. Sci., Polym. Symp.* **1978**, *63*, 59.
(6) Inaba, N.; Sato, K.; Suzuki, S.; Hashimoto, T. *Macromolecules* **1986**, *19*, 1690.
(7) Calahorra, E.; Cortazar, M.; Guzmán, G. M. *Polymer* **1982**, *23*, 1322.
(8) Martuscelli, E.; Pracella, M.; Yue, W. P. *Polymer* **1984**, *25*, 1097.
(9) Martuscelli, E.; Silvestre, C.; Addonizio, M. L.; Amelino, L. *Makromol. Chem.* **1986**, *187*, 1557.
(10) Alfonso, G. C.; Russell, T. P. *Macromolecules* **1986**, *19*, 1143.
(11) Briber, R. M.; Khoury, F. *Polymer* **1987**, *28*, 38.
(12) Inaba, N.; Yamada, T.; Suzuki, S.; Hashimoto, T. *Macromolecules* **1988**, *21*, 407.
(13) Li, Y.; Stein, M.; Jungnickel, B.-J. *Colloid Polym. Sci.* **1991**, *269*, 772.
(14) Huang, J.; Prasad, A.; Marand, H. *Polymer* **1994**, *35*, 1896.
(15) Balijepalli, S.; Schultz, J. M. *Macromolecules* **1996**, *29*, 6601.
(16) Wang, W.; Schultz, J. M.; Hsiao, B. S. *Macromolecules* **1977**, *30*, 4544.
(17) Svoboda, P.; Kressler, J.; Inoue, T. *J. Macromol. Sci., Phys.* **1996**, *B35*, 505.
(18) Kit, K. M. PhD Dissertation, University of Delaware, 1996.
(19) Kit, K. M.; Schultz, J. M. *J. Polym. Sci., Polym. Phys. Ed.* **1998**, *36*, 873.
(20) Kit, K. M.; Schultz, J. M. *Polymer* **1998**, *39*, 4969.
(21) Kit, K. M.; Schultz, J. M. *Int. J. Numer. Methods Eng.* **1997**, *40*, 2679.
(22) Hoffman, J. D.; Davis, G. T.; Lauritzen, J. I., Jr. In Hannay, M. B., Ed.; *Treatise on Solid State Chemistry*: *Crystalline and Noncrystalline Solids;* Plenum: New York, 1976.
(23) Wenig, W.; Karasz, F. E.; MacKnight, W. J. *J. Appl. Phys.* **1975**, *46*, 4194.
(24) Russell, T. P.; Stein, R. S. *J. Polym. Sci., Polym. Phys. Ed.* **1983**, *21*, 999.
(25) Russell, T. P.; Ito, H.; Wignall, G. D. *Macromolecules* **1988**, *21*, 1703.
(26) Martiscelli, E.; Canetti, M.; Seves, A. *Polymer* **1989**, *30*, 304.
(27) Runt, J. P.; Zhang, X.; Miley, D. M.; Gallagher, K. P.; Zhang, A. *Macromolecules* **1992**, *25*, 3902.
(28) Talibudden, S.; Wu, L.; Runt, J. *Macromolecules* **1996**, *29*, 7527.
(29) Stein, R. S.; Khambatta, F. B.; Warner, F. P.; Russell, T.; Escala; A.; Balizer, E. *J. Polym. Sci., Polym. Phys. Ed.* **1978**, *63*, 313.
(30) Oudhuis, A. A. C. M.; Thiewes, P. F.; van Hutten, P. F.; ten Brinke, G. *Polymer* **1994**, *35*, 3936.
(31) Cheng, S. Z. D.; Barley, J. S.; Von Meerwall, E. D. *J. Polym. Sci., Polym. Phys. Ed.* **1991**, *29*, 515.
(32) Hiemenz, P. C. *Polymer Chemistry*, 1st ed.; Marcel Dekker: New York, 1984.
(33) Keith, H. D.; Padden, F. J. *J. Appl. Phys.* **1964**, *35*, 1286.
(34) Tead, S. F.; Kramer, E. J. *Macromolecules* **1988**, *21*, 1513.
(35) Flynn, J. H. *Polymer* **1982**, *23*, 1325.
(36) Stasna, J.; De Kee, D. *Transport Properties in Polymers;* Technomic: Lancaster, PA, 1995.

MA020875T